Mon. Not. R. astr. Soc. (1980) **193**, 399–413

Absorption lines and ion abundances in the QSO PKS 0528 – 250

Donald C. Morton, Chen Jian-sheng*, Alan E. Wright† and Bruce A. Peterson
Anglo-Australian Observatory, Box 296, Epping, NSW 2121, Australia
David L. Jauncey *CSIRO Division of Radiophysics, Box 76, Epping, NSW 2121, Australia*

Received 1980 March 17; in original form 1980 January 2

Summary. Spectra of the QSO PKS 0528 – 250 ($z_e = 2.765$) have been obtained with the AAT at 2 Å resolution from 3100 to 7180 Å. Absorption line systems have been identified at $z_{A1} = 2.81322$, $z_{A2} = 2.81100$, $z_B = 2.53758$ and $z_C = 2.14077$. The ionization ranges from H I, Al II and Fe II to N V or O VI in system A, from H I and possibly Si II to C IV in B and from H I, Al II and Si II to C IV in C. In system A the Si IV and higher stages are concentrated in A2. Broad Lα profiles in A and C correspond to 2×10^{21} and 5×10^{20} atom cm^{-2} respectively. Column densities also have been estimated for several heavier elements at each redshift. In system A depletions by factors of 8 to 160 relative to solar abundances appear to be present in S II, O I and N I as well as the typical factor 10 for Si II and Fe II similar to interstellar clouds in the plane of our galaxy.

Longward of the Lα absorption in system A there are 44 lines of which only 27 have proposed identifications, whereas at the shorter wavelengths there are 112 lines of which 43 have plausible identifications due to one or more ions other than hydrogen. Thus caution is needed with the common assumption that most absorptions shortward of Lα emission in QSOs are due to Lα.

1 Preamble

A 19th magnitude stellar object was noted within the ± 7 arcsec positional uncertainty of the Parkes radio source 0528 – 250 by Bolton, Shimmins & Wall (1975). The images on the red and blue Palomar survey plates were of similar brightness. Coincidence to better than 3 arcsec was established with the NRAO interferometer by Condon, Hicks & Jauncey (1977). Two low resolution AAT spectra described by Wright *et al.* (1977) and Jauncey *et*

* Visiting astronomer from Peking Observatory, China.
† Present address: Australian National Radio Astronomical Observatory, Box 276, Parkes, NSW 2870, Australia.

al. (1978, hereinafter JWPC) had a strong absorption line system at $z_a = 2.812$ and several possible emission peaks, but no recognizable redshift system. Later observations at Lick by Smith, Jura & Margon (1979, hereinafter SJM) showed weak, but distinct peaks identifiable with Si IV λ 1397 + O IV] λ 1402, C IV λ 1549 and C III] λ 1909 giving the redshift $z_e = 2.765 \pm 0.01$. This is less than the main absorption redshift by 0.047! No Lα emission was found. A re-examination of the AAT spectra showed the C IV lines on both published plots and Si IV and C III] in one along with other maxima. The emission redshift is definitely established, though the line strengths may be variable. PKS 0528 − 250 must be classed as an unusual QSO rather than a BL Lac object.

The prominent absorption line system made this object a candidate for an AAT programme of higher resolution (~ 2 Å FWHM) observations of radio QSOs. A previous paper in this series by Wright *et al.* (1979) describes the QSO PKS 1157 + 014 at $z_e = 1.978$ which also has no Lα emission.

The optical coordinates of PKS 0528 − 250 from the Palomar Sky Survey are $05^h 28^m 05^s.19 \pm 0^s.07$, $-25° 05' 45'' \pm 0''.9$ (1950.0) and a finding chart has been provided by Condon *et al.* (1977). As noted by JWPC the light varies from about 17.5 to 19.5 mag. and the radio spectrum peaks between 1 and 3 GHz in the observer's frame with a steep decline towards lower frequencies. The identification of this type of QSO depends on discovery in a high frequency radio survey and an accurate radio position rather than an ultraviolet excess or strong emission lines detectable in a Schmidt objective prism survey.

2 Observations and data reduction

The spectra discussed here were obtained with the image-photon counting system and RGO spectrograph on the Anglo-Australian 3.9-m telescope. Data were collected on eight different nights: 1976 December 21, 1977 February 14, 15, 16, November 11, 12, December 16 and 1978 February 12. We used gratings of 1200 lines mm^{-1} in first order with dispersions of 33 Å mm^{-1} and effective blazes near 4600 and 6900 Å. The contribution of the sky was determined by placing the QSO in alternate apertures 20 arcsec apart and 2 or 3 arcsec diameter projecting to 1.6 and 2.4 Å respectively.

The data were reduced in the usual way except that no attempt was made to correct for the spectrograph and detector sensitivity variations with wavelength and position on the photocathode. It was found that using the flat field data produced more noise than it removed, probably due to registration problems.

After the wavelength scales were determined, the exposures in each band of about 1000 Å were summed and then these sums were combined to one continuous plot which is reproduced in Fig. 1. Correction factors were applied to each section indicated by the vertical dashed lines to produce a smooth continuum. Thus the ordinate does not represent observed counts and the continuum energy distribution is not reliable over large wavelength ranges. The data cannot be trusted for the measurement of emission-line profiles.

The resulting instrumental profile is about 2 Å FWHM. The corrections for the Earth's orbital motion were inadvertently omitted before summing. However, in each region the addition of the spectra is dominated to 87 per cent or more by contributions obtained at the same earth velocity. Thus we have reduced all observed wavelengths in Table 1 to a standard requiring a correction of -19.0 km s^{-1} which has been applied as the factor $(1-19/c)$ to all the derived redshifts $(1+z)$ to obtain the heliocentric values in the abstract.

A continuum level was estimated as shown in Fig. 1. The central wavelength λ_{obs} listed in Table 1 represents the line bisecting the area of each absorption line, and the equivalent width W_λ is this area expressed as the width of a totally absorbing rectangle. Thus W_λ/λ is

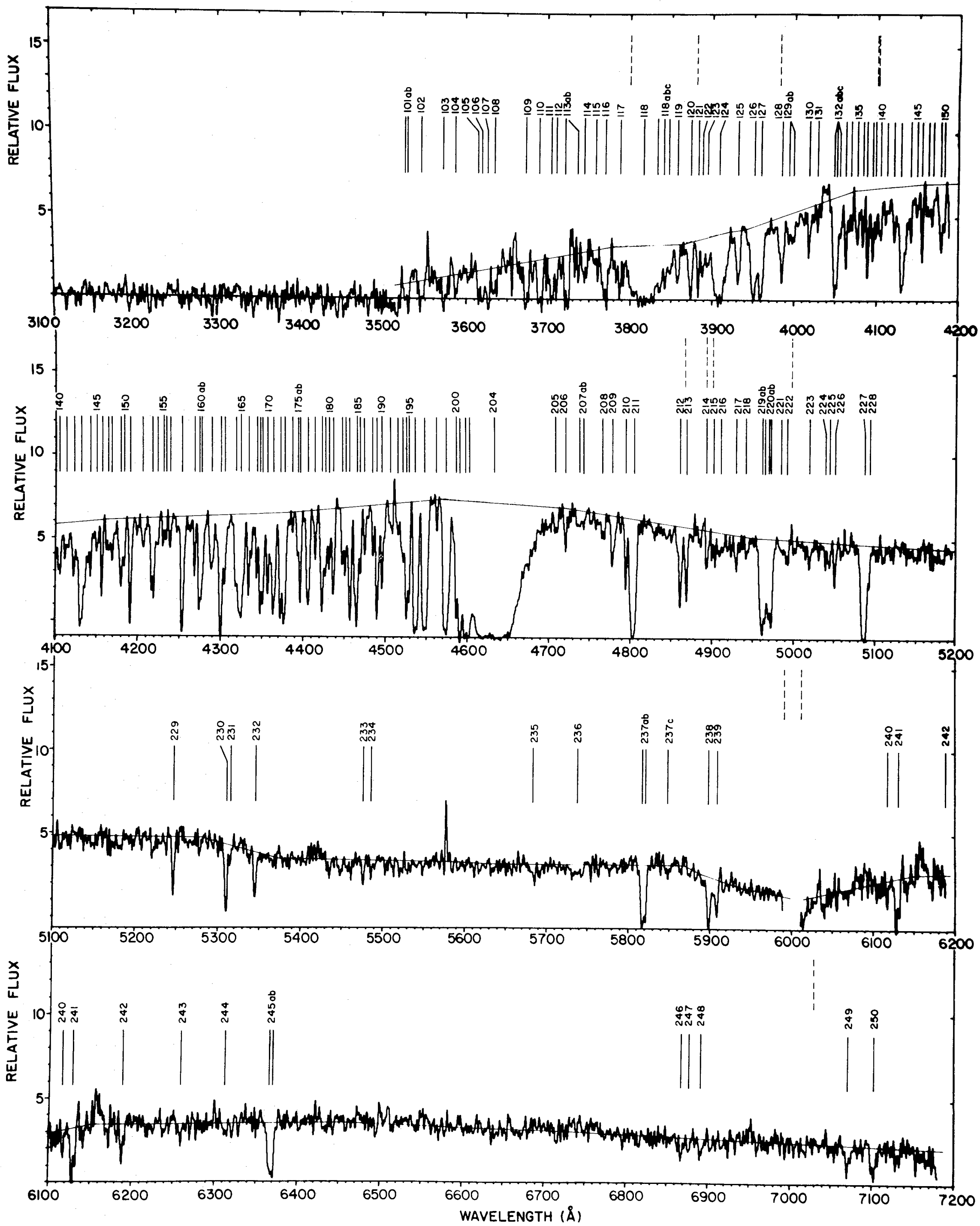

Figure 1. The spectrum of the QSO PKS 0528 – 250. Various exposures in bands of about 1000 Å have been summed after multiplication by factors to make the continuum moderately flat. Consequently the relative fluxes are unreliable over bands exceeding a few hundred Ångströms. The vertical dashed lines indicate where the pieces have been joined. Air wavelengths are plotted on the abscissa. The numbers label the lines in Table 1.

independent of redshift. For comparison with laboratory wavelengths λ_{lab}, all observed wavelengths have been converted to vacuum values using Edlèn's (1953, 1966) formula. The laboratory wavelengths and oscillator strengths of various ions are from the updated compilation by Morton (1978) or the list of N I lines by Lugger *et al.* (1978).

Table 1. Absorption lines in PKS 0528 – 250.

No.	air λ obs	vac λ obs	W_λ	Redshift System	Ion	vac λ lab	f	Δλ Obs–Calc	Notes
101a	3525.93	3526.94	3.45	A	O I	924.95	0.00159	+0.71	3 lines
				A	O I?	925.44	0.000354	−1.16	
				C	Fe III	1122.53	0.056	+1.11	
101b	3529.12	3530.13	6.07	A	H Iη	926.23	0.00318	−0.98	
102	3544.64	3545.65	8.22	A	O I	929.52	0.00236	+1.99	3 lines
				A	O I?	930.26	0.000537	−0.83	
				A	H Iζ	930.75	0.00481	−2.69	
103	3573.16	3574.18	7.41	A	O I	936.63	0.00374	+3.42	3 lines
				A	H Iε	937.80	0.00780	−1.04	
				A	O I?	937.84	0.000874	−1.19	
104	3587.48	3588.51	3.45	unident.					
105	3615.16	3616.19	3.34	A	O I	948.69	0.00645	−0.55	3 lines
106	3619.79	3620.83	5.78	A	H Iδ	949.74	0.01394	+0.09	
				C	P II	1152.81	0.236	−0.11	
107	3626.47	3627.50	6.63	A	O I	950.88	0.00157	+2.39	
				B	H Iβ	1025.72	0.07910	−1.29	
108	3634.50	3635.54	5.18	A	N I	953.41	0.0112	+0.81	
						953.65	0.0224	−0.11	
						953.97	0.0335	−1.33	
109	3673.38	3674.43	6.89	A	N I	963.99	0.0151	−0.64	A_1 components weak or absent
						964.63	0.0100	−3.08	
						965.04	0.00502	−5.04	
110	3690.31	3691.36	8.41	unident.					
111	3704.31	3705.37	6.20	A	O I	971.74	0.0148	+0.76	3 lines
				A	H Iγ	972.54	0.02899	−2.29	
112	3710.08	3711.13	3.14	unident.					
113a	3723.05	3724.11	7.19	A	O I	976.45	0.00330	+1.54	
				A	C III	977.03	0.768	−0.67	
113b	3737.40	3738.46	1.26	C	Si II	1190.416	0.251	−0.61	
114	3744.85	3745.92	3.15	unident.					
				C	Si II	1193.29	0.500	−2.17	
115	3759.91	3760.98	2.15	B	S IV	1062.67	0.0377	+1.47	
116	3770.13	3771.20	9.01	A	O I	988.7	0.051	+1.93	3 lines
				A	N III	989.79	0.107	−2.22	
				A	Si II	989.87	0.244	−2.53	
				C	N I	1199.55	0.133	+3.45	
						1200.22	0.0885	+1.34	
						1200.71	0.0442	−0.19	
117	3787.06	3788.14	6.61	C	Si III	1206.51	1.66	−1.47	
118	3817.5	3818.6	38:	C	H Iα	1215.67	0.4162	+0.2	
118a	3836.85	3837.94	5:	B	N II*?	1084.58	0.101	+0.88	absorption in wing of 118
118b	3842.92	3844.01	3:	unident.					
118c	3848.77	3849.86	3:	unident.					
119	3858.40	3859.49	2.37	A	S III	1012.50	0.0355	−0.51	
120	3873.85	3874.95	5.10	unident.					
121	3883.24	3884.34	2.68	unident.					
122	3888.82	3889.92	2.78	A	Si II	1020.70	0.0482	−1.42	
				C	N V?	1238.81	0.152	−1.14	
123	3895.28	3896.39	2.45	unident.					

No.	air λ obs	vac λ obs	W_λ	Redshift System	Ion	vac λ lab	f	Δλ Obs-Calc	Notes
124	3909.23	3910.34	16.79	A	H Iβ	1025.72	0.07910	-0.06	possible long λ unidentified component
				C	N V	1242.80	0.0757	+6.74	
125	3932.01	3933.13	3.71	A_2	O VI	1031.93	0.130	+0.20	
126	3950.63	3951.74	8.02	A	C II	1036.34	0.125	+0.85	
				A	C II*	1037.02	0.125	-2.85	
				A_2	O VI	1037.62	0.0648	-2.88	
127	3959.85	3960.97	7.76	A	O I	1039.23	0.00919	-0.94	
				C	Si II	1260.42	0.959	+2.03	
128	3985.27	3986.40	4.35	unident.					
129a	3994.08:	3995.21:	0.9:	A_2	Ar I	1048.22	0.230	+0.19	
b	3998.75:	3999.88:	1.8:	unident.					
sum	3997.22	3998.35	2.68						
130	4018.86	4019.99	1.61	A_2	Fe II?	1055.27	0.010	-1.90	
131	4029.05	4030.19	0.39	unident.					
132ab	4050.49	4051.64	7.14	A	S IV	1062.67	0.0377	+0.37	
				B	Fe II	1144.95	0.15	+1.03	
132c	4057.67	4058.81	1.59	unident.					
133	4063.31	4064.46	2.34	A_2	Ar I	1066.66	0.0594	-0.84	A_1 much weaker
134	4068.99	4070.14	1.56	unident.					may be double
135	4077.35	4078.50	2.25	B	P II	1152.81	0.236	+0.09	
136	4083.80	4084.95	1.58	unident.					
137	4089.69	4090.84	2.55	C	O I	1302.17	0.0486	+0.76	
138	4095.38	4096.53	2.34	C	Si II	1304.37	0.147	-0.46	strong rel to λ1190
139	4099.33	4100.48	1.49	unident.					
140	4104.79	4105.94	2.11	unident.					
141	4112.89	4114.05	1.68	unident.					
142	4122.00	4123.16	1.92	unident.					
143	4132.21	4133.37	8.67	A	N II	1083.99	0.101	+0.82	
				A	N II*?	1084.58	0.101	-1.43	
				A	N II**?	1085.54	0.0161	-5.09	
						1085.70	0.0845	-5.70	
144	4142.62	4143.78	1.66	unident.					
145	4149.86	4151.03	1.09						
146	4156.04	4157.21	1.70						
147	4164.01	4165.19	1.54						
148	4169.27	4170.44	1.27						
149	4179.30	4180.48	3.05	A	Fe II	1096.89	0.037	-1.25	
150	4183.38	4184.56	0.85	unident.					
151	4190.63	4191.81	3.16	C	C II	1334.53	0.118	+0.09	C II* absent

No.	air λ obs	vac λ obs	W_λ	Redshift System	Ion	vac λ lab	f	Δλ Obs-Calc	Notes
152	4206.20	4207.39	1.10	unident.					
153	4217.38	4218.57	3.40	unident.					
154	4222.58	4223.76	1.12	unident.					
155	4229.82	4231.01	0.51	unident.					
156	4232.84	4234.03	0.49	unident.					
157	4238.26	4239.45	0.75	unident.					
158	4253.25	4254.44	4.58	unident.					
159	4267.77	4268.97	1.27	B	Si III	1206.51	1.66	+0.58	
160a	4273.53	4274.73	3:	A_2	Fe II	1121.99	0.020	-1.44	
b	4276.87	4278.07	2:	A_2	Fe III	1122.53	0.056	-0.16	
sum	4275.30	4276.50	4.95						
161	4288.53	4289.74	2.58	unident.					
162	4299.15	4300.35	5.32	B	H Iα	1215.67	0.4162	-0.45	
163	4304.27	4305.48	2.64	unident.					
164	4317.25	4318.46	2.15:	A_2	Fe II	1133.68	0.0063	-2.27	
165	4323.48	4324.70	7.14	A	N I	1134.16	0.0134	+0.89	
						1134.42	0.0268	-0.11	
						1134.98	0.0402	-2.24	
166	4333.99	4335.21	3.19	unident.					
167	4342.84	4344.06	1.62	unident.					
168	4347.21	4348.43	2.77	unident.					
169	4350.80	4352.03	2.44	unident.					
170	4356.34	4357.57	2.33	A	Fe II	1143.24	0.015	-0.82	
						1142.38	0.0069		
171	4363.27	4364.49	4.90	A	Fe II	1144.95	0.15	-0.46	
172	4372.16	4373.39	3.99	unident.					
173	4376.96	4378.19	4.45	C	Si IV	1393.75	0.528	+0.46	
174	4386.55	4387.78	0.40	unident.					
175a	4392.33	4393.57		A_2	P II	1152.81	0.236	-0.06	weaker
b	4395.64	4396.88		A_1	P II	"	"	+0.68	
sum	4395.17	4396.41	3.14						
176	4405.34	4406.57	3.60	C	Si IV	1402.77	0.262	+0.51	
177	4413.99	4415.23	1.08	unident.					
178	4422.52	4423.75	3.34	B	S II	1250.59	0.00535	-0.59	
179	4426.73	4427.97	1.99	unident.					
180	4431.03	4432.27	1.52	unident.					
181	4436.13	4437.37	2.46	B	S II	1253.81	0.0107	+1.64	
182	4447.04	4448.28	1.19	unident.					
183	4450.41	4451.65	1.76	unident.					
184	4456.18	4457.43	3.71	B	S II	1259.52	0.0159	+1.50	
				B	Si II	1260.42	0.959	-1.68	
				B	Fe II	1260.54	0.020	-2.11	

No.	air λ obs	vac λ obs	W_λ	Redshift System	Ion	vac λ lab	f	Δλ Obs-Calc	Notes
185	4464.17	4465.42	4.84						
186	4468	4470.17	1.36	unident.					
187	4474.60	4475.85	1.27						
188	4484.28	4485.53	1.18						
189	4489.64	4490.89	3.79						
190	4495.78	4497.04	2.16						
191	4506.12	4507.38	0.95	unident.					
192	4514.77	4516.04	0.87						
193	4520.07	4521.33	2.01						
194	4524.95	4526.22	3.55						
195	4528.18	4529.45	2.04						
196	4536.54	4537.81	7.03	A	S III	1190.21	0.0224	+0.31	
				A	Si II	1190.42	0.251	-0.49	
197	4547.44	4548.71	7.81	A	Si II	1193.29	0.500	-0.53	
198	4562.14	4563.42	0.46	A_2	Si II*?	1197.39	0.125	-0.12	Si II* λ1264.7 absent
199	4573.34	4574.62	8.27	A	N I	1199.55	0.133	+1.51	
						1200.22	0.0885	-1.04	
						1200.71	0.0442	-2.91	
200	4585.96	4587.24	2.66	unident.					
201	4590.94	4592.23	6.07						
202	4596.50	4597.78	4.35	A_2	Si III	1206.51	1.66	-0.52	broad line, two
				A_1				-3.20	minima with
203	4601.73	4603.02	5.82	unident.				+2.04	A_1 between
204	4633.06	4634.36	70.50	A	H Iα	1215.67	0.4162	-0.20	
205	4708.69	4710.00	0.70	unident.					
206	4720.00	4721.32	0.94	A_2	N V	1238.81	0.152	-0.08	
207a	4736.37	4736.4	1.12	A_2	N V	1242.80	0.0757	+1.1	
b	4742.35	4742.4		unident.					
208	4766.29	4767.62	1.00	A	S II	1250.59	0.00535	-0.07	
209	4778.02	4779.35	2.14	A	S II	1253.81	0.0107	-0.61	
210	4794.17	4795.52	2.08	C	Si II?	1526.71	0.0764	+0.17	
211	4803.08	4804.42	9.24	A	S II	1259.52	0.0159	+2.69	
				A	Si II	1260.42	0.959	-0.74	
				A	Fe II	1260.54	0.020	+0.20	
212	4861.01	4862.36	2.42	C	C IV	1548.19	0.194	-0.46	
213	4868.61	4869.97	1.77	C	C IV	1550.76	0.0970	-0.92	
214	4893.94	4895.31	1.20						
215	4902.75	4904.12	1.18	unident.					
216	4910.16	4911.53	1.55						
217	4929.64	4931.01	1.22	B	Si IV	1393.75	0.528	+0.20	
218	4942.58	4943.95	0.74	unident.					

No.	air λ obs	vac λ obs	W_λ	Redshift System	Ion	vac λ lab	f	Δλ Obs-Calc	Notes
219a	4960.74	4962.12	5.2	A_2	O I	1302.17	0.0486	-0.76	
b	4964.88	4966.26	2.65	A_1				+0.49	
sum	4962.15	4963.53	7.85	B	Si IV	1402.77	0.2262	+0.81	
220a	4968.74	4970.12		A_2	Si II	1304.37	0.147	-1.15	
b	4973.23	4974.61		A_1				+0.45	
sum	4971.19	4972.57	6.72	A				-0.14	
221	4986.29	4987.68	0.85	unident.					
222	4992.07	4993.46	0.95	unident.					
223	5019.78	5021.18	1.22	unident.					
224	5039.13	5040.53	0.80	unident.					
225	5043.81	5045.22	1.10	unident.					
226	5050.74	5052.14	1.36	C	Fe II	1608.46	0.22	+0.01	
227	5086.43	5087.84	8.73	A	C II	1334.53	0.118	+0.14	
				A_2	C II*	1335.70	0.118	-2.83	
228	5092.70	5094.12	1.19	A_1	C II*	1335.70	0.118	+0.48	
229	5246.36	5247.82	1.91	C	Al II	1670.79	1.88	-0.08	
230	5309.85	5311.32	3.12	A_2	Si IV	1393.75	0.528	-0.59	
231	5314.47	5315.95	1.00	unident.					
232	5344.92	5346.41	2.65	A_2	Si IV	1402.77	0.262	+0.12	
233	5475.85	5477.37	0.78	B	C IV	1548.19	0.194	+0.18	
234	5485.36	5486.89	0.41	B	C IV	1550.76	0.0970	+0.61	
235	5684.26	5685.83	1.34	unident.					
236	5736.26	5737.85	2.27	unident.					
237a	5817.10	5818.71	4.50	A_2	Si II	1526.71	0.0764	+0.05	
b	5821.00	5822.61	3.00	A_1				+0.56	
237c	5848.04	5849.66	1.27	A_1	Si II*?	1533.43	0.0760	+1.99	Si II* λ1264.7 absent
238	5898.95	5900.58	5.61	A_2	C IV	1548.19	0.194	+0.06	
239	5907.69	5909.33	3.37	A_2	C IV	1550.76	0.0970	-0.99	
				B	Al II	1670.79	1.88	-1.59	
240	6117.47	6119.16	1.29	unident.					
241	6128.17	6129.86	3.5:	A_2	Fe II	1608.46	0.22	-0.37	
	6131.36	6133.06	2.1:	A_1				-0.74	
sum	6129.00	6130.70	5.56	A					
242	6188.42	6190.14	2.57	unident.					
243	6258.96	6260.69	1.21	unident.					
244	6312.73	6314.47	1.15	A_2	C I	1656.93	0.136	-0.49	
245a	6366.75	6368.51		A_2	Al II	1670.79	1.88	+0.73	
b	6370.41	6372.17		A_1				+0.68	
sum	6368.08	6369.83	8.00	A				+0.19	
246	6868.09	6869.98	1.82	unident.					atmospheric O_2 B band
247	6876.73	6878.63	0.88	unident.					atmospheric O_2 B band
248	6891.62	6893.52	1.69	A	Si II?	1808.01	0.00371	0.75	atmospheric O_2 B band
249	7070.40	7072.35	3.62	A_1	Al III	1854.72	0.539	-0.55	
250	7101.64	7103.60	4.43	A_1	Al III	1862.79	0.268	-0.07	too strong

Table 1 lists the lines we believe to be real considering the noise in each region of the spectrum. Our equivalent widths, on the whole, tend to be smaller than those of SJM, presumably because their lower resolution (7 or 5 Å) resulted in more blended lines.

3 Redshift systems

Like many QSOs the number of absorption lines is much larger on the short wavelength side of the expected position for Lα emission at 4577 Å. Absorption redshifts in 0528 – 250 were searched for systematically using the scheme described by Wingert (1975). The search list was the same but the range was $z = 0$ to 4.0 and the interval was $\Delta z = 0.0005$. The permitted wavelength errors were ± 2.0 Å for the two broad lines at 3818 and 4633 Å and ± 1.0 Å for all the rest. A redshift was considered possible if five or more lines were identified, of which at least two had $W_\lambda \geqslant 1.3$ and at least two more had $W_\lambda \geqslant 1.0$. This latter value exceeds the detection limit of about 0.8 Å except where the extreme overlapping may require a line to have a larger equivalent width to be seen. Lα had to be present with $W_\lambda \geqslant 1.3$ if accessible between 3521 and 7175 Å and if W_λ(Lα) $\geqslant$ 7.4, Lβ also had to be present if accessible. Then, of course, we applied the basic physical constraints that line strengths of an ion had to increase with oscillator strength. We also considered the possibility that the hydrogen would be almost fully ionized and relaxed the criterion that Lα and Lβ had to be present if accessible.

In all cases vacuum wavelengths were used. A question mark following the ion label in Table 1 indicates an uncertain identification due to poor wavelength coincidence, a weak feature, or a blend. When a line is wide, a wavelength error exceeding the usual ± 1.0 Å limit has been accepted.

The search turned up three definite systems, and examination of some longer wavelength lines showed that one system has two components. Averaging the good identifications in each case gave the following redshifts (a) used for calculating $\Delta\lambda = \lambda_{obs} - (1 + z)\lambda_{lab}$ in Table 1 and (b) corrected to the heliocentric standard.

	A1	A2	Mean A	B	C
(a)	z = 2.91346	2.81124	2.81235	2.53780	2.14097
(b)	z = 2.81322	2.81100	2.81211	2.53758	2.14077
	ΔV = + 3815	+ 3640	+3728	− 18654	− 53759

Radial velocities ΔV relative to the emission lines at $z_e = 2.765$ also are listed. No other redshift systems could be identified with certainty. We also compared plots of the QSO spectrum and the standard lines on a logarithmic scale but found no more systems.

$z_A = 2.81211$

This system is responsible for the strong H I Lα line at 4633 Å as well as Lβ at 3909 Å and probably higher members to Lη, though some are blended with other species. As already noted by JWPC and SJM, numerous low ionization species typical of interstellar H I clouds are present at z_A. Specifically we found C II, N I, O I, Al II, Si II, P II, S II, Ar I and Fe II. Also C I may be present but λ1657 needs confirming and λλ 1560 and 1329 should be searched for. Higher ions such as C III, N II, N III, Si III, S III, S IV and Fe III probably occur but their identifications depend on single lines in the crowded region shortward of Lα. More certain are the doublets of C IV, N V, Al III and Si IV. The stronger component of O VI can be identified with a line if we assume that the other O VI line is blended with C II at the same redshift.

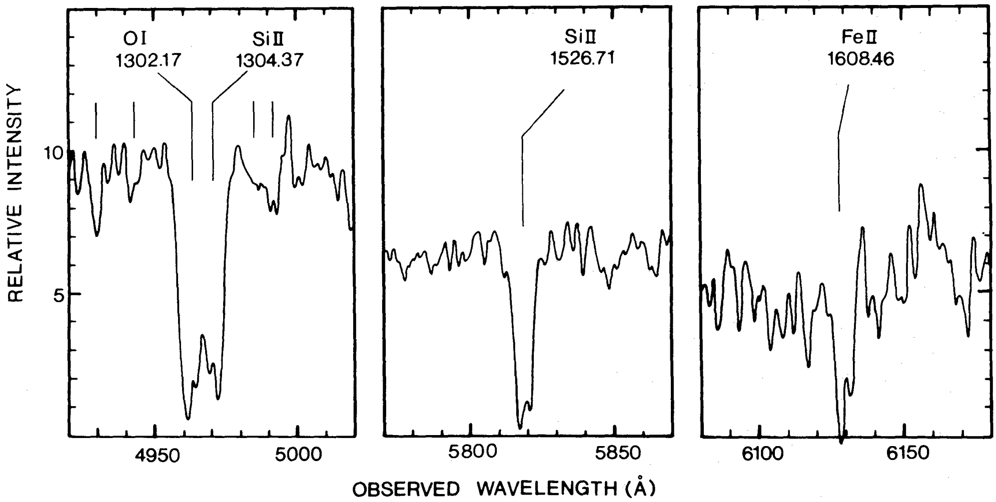

Figure 2. Expanded plots showing the double components of four strong absorption lines. The four additional vertical bars in the first rectangle indicate weak features also listed in Table 1.

$z_{A1} = 2.81322$, $z_{A2} = 2.81100$

In the A system the line of Fe II λ1608 (No. 241) is clearly double, and O I λ1302 (No. 219) as well as Si II λλ1304, 1527 (Nos 220, 237) also seem to have two minima as shown in Fig. 2. We have used these lines to determine the redshifts z_{A1} and z_{A2} listed above. Most other z_A lines are unresolved blends, but the line centres of the higher ions C IV, N V and Si IV are best accounted for by z_{A2}. The line centres for Lyman γ, ϵ, ζ and η suggest that A2 component may be stronger in H I, as is the case for Fe II λ1608 and possibly λλ1143, 1122. A2 also may be stronger in Ar I, but it is weaker in P II. The components have about equal strength in O I and Si II. Absorption from the excited fine structure level of C II* in the A1 component could explain a feature on the edge of the C II profile. N II* and N II** at both redshifts could be present in the wing of the N II line. Although Si II* λ1197 in A2 fits a line very well, the absence of the strongest line at λ1265 rules out this excited level. The two components A1 and A2 are separated by 175 km s^{-1} and the mean A is 3728 km s^{-1} to the *red* of the emission line system.

$z_B = 2.53758$

Lα and Lβ are relatively insignificant features, the C IV doublet is weak and one component of Si IV is lost in a blend. Nevertheless there are enough identifications in this system to leave very little doubt about its reality. Al II, Si II, Si III, P II, S II and possibly Fe II and S IV seem to be present as well as C IV and Si IV.

$z_C = 2.14077$

This system has a conspicuous Lα absorption at 3818 Å and a strong C IV pair at 4861 and 4869 Å. Also probably present are C II, N I, O I, Al II, Si II, Si III, Si IV, P II and perhaps Fe III.

In the crowded region shortward of 4630 Å, some of the line identifications in Table 1 could be chance coincidences. However, in many cases, such as O I in system A, the definite presence of one line implies that other lines of larger or comparable oscillator strength also must occur.

4 Column densities

Many sources of error hinder the reliable determination of column densities from absorption lines like those we have in 0528 – 250. The signal is noisy in many regions, the continuum level is uncertain where numerous lines overlap, identifications can be wrong, blending often distorts a line and sometimes another line can contribute without being suspected. When lines are strong enough to show damping wings, as in the first two Lyman lines in system A, profiles can be fitted with the result that $N(\text{H I}) = 2.2 \times 10^{21}\,\text{cm}^{-2}$ from Lα (both wings) and 1.5×10^{21} from Lβ (red wing). Thus we agree with $3 \pm 1 \times 10^{21}\,\text{cm}^{-2}$ obtained by SJM for Lα but not with JWPC whose formula is in error by a factor 4.5. In system C, Lα has an extended red wing which we attribute to blends of other lines. The blue side approximates a damping profile with $N(\text{H I}) = (5 \pm 1) \times 10^{20}\,\text{cm}^{-2}$.

For most other lines we must depend on equivalent widths, usually with significant errors, and a curve of growth based on the simplifying assumption of a Maxwellian distribution of velocities described by the single parameter $b = 2^{1/2}\sigma_x$. Even then it is difficult to estimate the effects of saturation unless at least one line is weak enough to be close to the linear region. This may be the case for C IV in B and S II in A, where the slope determined by the two observed lines of each ion implies little saturation. In other ions, the observed widths of a line indicate an upper limit such as $b \leqslant 120\,\text{km s}^{-2}$ for N V in A. Even when there are multiple absorbing clouds, representation by a single velocity distribution may be a good approximation for species of similar ionization potential, as sometimes occurs along interstellar sight lines (Morton 1975, 1978).

As shown in Fig. 3 for system A, Si II, S II and O I fit on a curve with $b = 150\,\text{km s}^{-1}$ where the relatively weak line of S II λ 1251 fixes the absolute column density. As some indication of the uncertainties in the derived column densities, we also have considered the curve with $b = 120\,\text{km s}^{-1}$ which is an acceptable fit for Si II and S II and slightly better for O I. Since the N I lines are blends of three transitions, they lie on a separate curve above that for Si II, S II and O I. It is noteworthy that Fe II, which has nearly the same ionization potential as Si II, lies on a lower curve with $b = 80\,\text{km s}^{-1}$ in Fig. 2, where only the four reliable lines $\lambda\lambda$ 1055, 1097, 1145 and 1608 are plotted. Perhaps the Fe II is depleted relative to Si II in some clouds. The presence of the dual curves precludes fitting single lines such as Al II and leaves considerable uncertainty in the whole procedure.

Our best estimates for the ranges of velocity parameters b and column densities N are listed in Table 2. Our results for H I, Si II and S II in system A are in reasonable agreement with SJM. However, for Al III, our spectrum has the equivalent widths reversed, as if there were an unidentified line contributing to λ 1863, whereas SJM found $W_\lambda(1855) = 5.1$ and

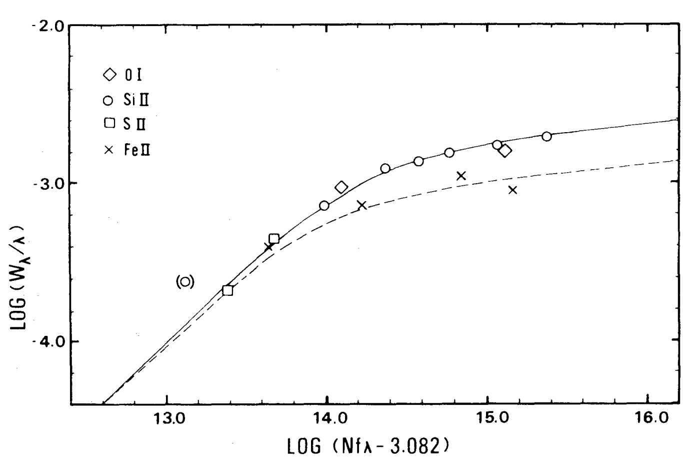

Figure 3. Curve of growth for lower ion stages in system A. The effect of a simple Maxwellian velocity distribution is shown by a solid line for $b = 150\,\text{km s}^{-1}$ and a dashed line for $b = 80\,\text{km s}^{-1}$. The circle in parentheses represents λ 1808 of Si II which is unreliable due to blending with telluric O_2.

Table 2. Column densities towards PKS 0528 – 250.

System	Ion	log N (cm^{-2})	b (km s^{-1})	log N (cm^{-2})	log(N/N$_{H\,I}$)	log(N/N$_H$)$_o$	Difference
		SJM*	This Paper				
A	H I	21.5±0.2	damped	21.27±0.08			
	C I		≤ 80	≤ 14.7	≤ -6.6		
	O I		150-120	16.38-16.54	-4.8±0.1	-3.17	-1.6±0.1
	N I		150-120	15.10-15.20	-6.1±0.1	-3.94	-2.2±0.1
	Al III	14.1±0.2			-7.2±0.2	-5.60	-1.6±0.2
	Si II	16.1±0.5	150-120	15.38-15.66	-5.75±0.15	-4.45	-1.3±0.15
	S II	15.6±0.2	150-120	15.55±0.01	-5.7±0.1	-4.79	-0.9±0.1
	Fe II		80-60	15.71-15.90	-5.5±0.2	-4.60	-0.9±0.2
A2	C IV		∞-150	14.55-14.77	(-6.6±0.1)	-3.43	(-3.2±0.1)
	N V		120-50	14.12-14.25	(-7.05±0.1)	-3.94	(-3.1±0.1)
	Si IV		70-50	14.45-15.31	(-6.4±0.4)	-4.45	(-2.0±0.4)
B	H I		≥ 40	16.4±2.0			
	C IV		∞-40	13.73-13.81	-2.6±2.0	-3.43	+0.8±2.0
	Si IV		∞-40	13.58-13.83	-2.7±2.0	-4.45	+1.7±2.0
C	H I		damped	20.70			
	C IV		80-50	14.57-14.79	-7.0±0.1	-3.43	-3.6±0.1
	Si IV		120-80	14.64-15.08	-5.8±0.2	-4.45	-1.4±0.2

* Smith, Jura, Margon (1979)

$W_\lambda(1863) = 2.7$ Å in a region which they re-observed at 5 Å resolution. Thus we have adopted their result in Table 2. In system B, the upper limit for H I was determined by the absence of damping wings. For the higher ions in Table 2, the doublet ratio fixed the range of b except for N V in A2 where the upper limit was obtained from the observed width and the lower limit from Si IV. Ratios to the H I density are quoted and comparisons are made with the solar abundances of Withbroe (1971). Parentheses are used for the A2 ions as a reminder that it was necessary to use the total H I for system A. The last column lists the logarithmic depletion of the ion relative to the solar element abundance.

The spectrum drops to an undetectable flux shortward of 3520 Å (air) whereas the Lyman limit for system A is at 3475 Å. Presumably the superposition of Lyman lines near the limit increases the effective cutoff wavelength. For $N_{\rm H\,I} = 1.8 \times 10^{21}$ cm^{-2} the optical depth at the Lyman limit is about 1200.

The strong Lα absorption line in system A prompted a search for redshifted 21 cm absorption with the Parkes 64-m telescope by Bolton *et al.* (1979). Unfortunately at 372.6 MHz the continuum flux density of PKS 0528 – 250 is only about 0.2 Jy so that no line was detected above an equivalent width limit (W_ν) of about 10 kHz. If we assume a mean spin temperature for the gas of 100 K, then our result implies that the H I column density is less than about 4×10^{20} cm^{-2}. This value is mildly inconsistent with N(H I) = $(19 \pm 4) \times 10^{20}$ cm^{-2} deduced from the Lα and Lβ lines. If we adopt the latter value our equivalent width limit implies a spin temperature greater than 500 K. Although still compatible with hot, neutral gas in a galaxy such as our own, this spin temperature seems more likely in gas located near the QSO. It should be noted that 0528 – 250 is unique among known QSOs in having two very broad Lα lines. Clearly H I absorption also should be searched for at 452.2 MHz.

5 Discussion

The location and nature of the regions producing the absorption lines in QSOs continue to receive considerable attention in the literature. Weymann *et al.* (1979) have proposed three types of regions: (i) gas ejected from the QSO; (ii) gas in clouds associated with the QSO; and (iii) gas in intervening clouds not related to the QSO. The ejected material typically has velocities from 0 to 20 000 km s^{-1} with respect to the QSO emission lines, whereas the associated clouds may range from –3000 to +3000 km s^{-1}. These clouds could be contained in a cluster of galaxies around the QSO and the intervening clouds could be in galaxies between the Sun and the QSO. The abrupt increase in absorptions around the Lα emission and on the blue side usually is attributed to H I clouds where the heavy elements are either absent or have undetectably small equivalent widths.

In 0528 – 250 none of the absorption line systems has the wide and often asymmetric profiles usually associated with a QSO wind. Both systems B and C could be formed by ejection, but their narrow symmetric lines leave them indistinguishable from an intervening cloud. Since A1 and A2 exceed the emission-line redshift, they presumably are due to clouds related to the QSO, though the velocities of + 3815 and + 3640 km s^{-1} relative to the QSO are rather large for a normal cluster of galaxies. Other examples are PHL 1222 where Williams & Weymann (1976) found an absorbing cloud with $N(\text{H I}) = 2 \times 10^{20}\ \text{cm}^{-2}$ approaching the emission line region at 3200 km s^{-1} and 1557 – 199 where White, Murdoch & Hunstead (1980) found a relative velocity of 15 000 km s^{-1}; PKS 0528 – 250 is specially interesting because the large H I column density of $2 \times 10^{21}\ \text{cm}^{-2}$ implies a galaxy similar to our own with a velocity component of 3700 km s^{-1} towards the QSO.

The broad hydrogen Lα lines with damping wings in both A and C and the low ion states of heavier elements are suggestive of interstellar clouds in the plane of our own Galaxy. At the same time the higher ion states of C IV, N V and Si IV could be formed in a galactic halo. Thus it is useful to compare our equivalent widths with the *IUE* data towards HD 38282 in the LMC where Savage & de Boer (1979) have attributed many features to the halo gas in our Galaxy. Our C IV and Si IV lines are comparable in system B, but 3 to 12 times stronger in A2 and C, and N V in A2 is about 10 times the upper limit for the halo. The strongest halo line plotted by Savage & de Boer is C II λ 1334.5 which is saturated over 160 km s^{-1}. According to de Boer, Koornneef & Savage (1980) other low ions including Al II and Si II in this star and O I and Si II in HD 38268 also have remarkably wide profiles. The low ionization absorption lines in PKS 0528 – 250 have similar widths in systems B and C but O I and C II in A are considerably wider. Also the velocity parameter $b = 80$–150 km s^{-1} for the lower ions of system A is 10 or more times what is usually found on a galactic line of sight.

Although the column densities in Table 2 are not very reliable, it does seem that the abundances of all the ions measured are significantly depleted compared with the Sun. However in interstellar H I clouds (Morton 1975, 1978) O I and N I usually are depleted by 1.0 dex or less while S II is undepleted in contrast with the significantly lower abundances of these ions in system A. In PHL957, Wingert (1975) found N I, O I, Si II, S II and Fe II down by 1.0 dex or more, somewhat like 0528 – 250. The ratio Al III/H I in Table 2 is large compared with ζ Oph but actually slightly smaller than found towards ζ Pup. As noted by SJM, the similarity of the depletion of Si II and S II implies no ordinary grains in the A cloud, consistent with the absence of a redshifted 2200 Å absorption.

The upper limit $\log N(\text{C I}) \leqslant 14.7$ in system A quoted in Table 2 is based on the possible identification of λ1657 with line number 244. Unfortunately the other strong C I lines are either lost in blends or, in the case of λλ1560 and 1329 just below the detection limit. If C I is present with the above column density, the ratio to hydrogen nuclei is −6.6 dex, intermediate between −5.8 and −7.2 found in ζ Oph and ζ Pup respectively (Morton 1975, 1978).

Among the higher ions, it is unusual in our Galaxy to find N V as strong relative to C IV as occurs in system A2. Also in A2, B and C, the abundance of Si IV is equal to or greater than C IV, unlike what Savage & de Boer (1979) found for our halo in the direction of the LMC.

Thus systems A and C have the wide Lα lines expected for an intervening galaxy but C IV and Si IV seem rather stronger and system A also has unusually strong O I and C II. In contrast system B has a relatively narrow Lα line and no detectable N I or O I, but reasonable C IV and Si IV. Perhaps the line-of-sight at B passes through the halo but not the disc of a galaxy. Further comparisons will be useful when more data are obtained on the UV absorptions in our halo.

The pattern of identified lines in PKS 0528 − 250 is worth noting in view of the usual assumption for high redshift QSOs that most of the lines on the short wavelength side of the Lα emission are due to Lα absorption. The Lα emission should occur at 3.765 × 1215.67 = 4577 Å, but we have adopted a separation at 4700 Å, where Fig. 1 shows a significant change in the line density. Each entry in Table 1 with a separate wavelength and equivalent width was counted as a line except when the splitting was due to the two components of system A. In two cases, one on each side of 4700 Å, where a single identified line was suspected of having an unidentified component the line was counted as identified. At the same time, the two questionable identifications of Si II*, also on each side of 4700 Å were rejected. Thus shortward of 4700 Å there are 112 lines in Table 1 of which three are definitely Lα absorption, 43 have plausible identifications due to one or more heavier elements, one is Lη and six are blends of higher Lyman lines with heavier species. Longward of 4700 Å but excluding the telluric *B* band there are 44 lines of which 27 have plausible identifications. Thus 38 per cent of the lines shortward of 4700 Å and 61 per cent of the longer wavelength lines are identified with transitions other than Lα or higher Lyman lines.

If we make the plausible assumption that the unidentified lines longward of 4700 Å are not Lα absorption and, further, that the same fraction of non-Lα, non-identified lines occurs *shortward* of 4700 Å, then only a small fraction (~ 20 per cent) of all the shortward lines can be due to H I Lyman absorption. We are aware that the equivalent widths shortward of 4700 Å, excluding the two strong Lα lines, are on the average a factor 2 larger than longward of this wavelength. However, the ratio of mean equivalent widths for the identified to unidentified lines is approximately the same (~ 2.7) either side of the 4700 Å boundary. Nevertheless there remains a concern that some of the lines longward of the boundary may not be real because many of them are relatively weak. Additional observations would be worthwhile to confirm these lines.

The exact percentages could change with different criteria for counting lines and the reliability of their identifications. Certainly further observations of 0528 − 250 longward of 4700 Å would be useful to establish firmly the fraction of unidentified lines stronger than a particular equivalent width limit. Even so, one important conclusion is clear from this QSO. In any statistical study of QSO absorption lines it can be dangerous to neglect the contributions of heavy elements shortward of the Lα emission. Also it is a risk to assume that all identified lines on the blue side of the Lα emission are Lα absorption when there are unidentified lines on the red side.

Acknowledgments

We wish to thank John Bolton for helpful comments on the line identifications and Peter Krug for assistance in the reduction of the spectra. Chen Jian-sheng gratefully acknowledges the hospitality of the Anglo-Australian Observatory.

References

Bolton, J. G., Shimmins, A. J. & Wall, J. V., 1975. *Aust. J. Phys. Astrophys. Suppl., No. 34,* 11.

Bolton, J. G., Jauncey, D. L., Murray, J. D., Peterson, B. A., Savage, A. & Wright, A. E., 1979. Private communication.

Condon, J. J., Hicks, P. D. & Jauncey, D. L., 1977. *Astr. J.,* **82**, 692.

de Boer, K. S., Koornneef, J., Savage, B. D., 1980. *Astrophys. J.,* **236**, 769.

Edlèn, B., 1953. *J. Opt. Soc. Am.,* **43**, 339.

Edlèn, B., 1966. *Metrologia,* **2**, 71.

Jauncey, D. L., Wright, A. E., Peterson, B. A. & Condon, J. J., 1978. *Astrophys. J.,* **221**, L109.

Lugger, P. M., York, D. G., Blanchard, T. & Morton, D. C., 1978. *Astrophys. J.,* **224**, 1059.

Morton, D. C., 1975. *Astrophys. J.,* **197**, 85.

Morton, D. C., 1978. *Astrophys. J.,* **222**, 863.

Savage, B. C. & de Boer, K. S., 1979. *Astrophys. J.,* **230**, L77.

Smith, H. E., Jura, M. & Margon, B., 1979. *Astrophys. J.,* **228**, 369.

Weymann, R. J., Williams, R. E., Peterson, B. M. & Turnshek, D. A., 1979. *Astrophys. J.,* **234**, 33.

Williams, R. E. & Weymann, R. J., 1976. *Astrophys. J.,* **207**, L143.

Wingert, D. W., 1975. *Astrophys. J.,* **198**, 267.

Withbroe, G. D., 1971. *The Menzel Symposium NBS Special Publ.,* **383**, ed. Gebbie, K. B., U.S. Government Printing Office, Washington.

Wright, A. E., Jauncey, D. L., Peterson, B. A. & Condon, J. J., 1977. *Astrophys. J.,* **211**, L115.

Wright, A. E., Morton, D. C., Peterson, B. A. & Jauncey, D. L., 1979. *Mon. Not. R. astr. Soc.,* **189**, 611.

White, G. L., Murdoch, H. S. & Hunstead, R. W., 1980. *Mon. Not. R. astr. Soc.,* **192**, 545.